

Electronic Effects of Ligand Substitution on Metal Organic

Frameworks Photocatalysts: The Case Study of UiO-66

*Lijuan Shen, Ruowen Liang, Mingbu Luo, Fenfen Jing and Ling Wu**

State Key Laboratory of Photocatalysis on Energy and Environment,

Fuzhou University, Fuzhou 350002 (P.R. China)

*Corresponding Author. Tel.: +86 591 83779105; E-mail: wuling@fzu.edu.cn

Preparations

All chemicals were obtained commercially and used without further purification.

Synthesis of UiO-66(1), UiO-66-NH₂ (2), UiO-66-NO₂ (3), and UiO-66-Br (4). Sample UiO-66 was synthesized by a modified method reported in literature.¹ In a typical synthesis, ZrCl₄ (0.2332 g, 1.0 mmol) and terephthalic acid (H₂BDC) (0.1661 g, 1.0 mmol) were dissolved in DMF (50 mL), subsequently, the solution was transferred to a 100 mL Teflon-lined stainless steel autoclave. The autoclave was sealed and heated in an oven at 120 °C for 48 h under autogenous pressure, after cooled naturally, the sample was purified with anhydrous methanol for several times to make sure that the occluded DMF molecules were eliminated, followed by drying under vacuum (100 °C, 12 h) before using the samples for the photocatalytic reactions. UiO-66-NH₂ (2), UiO-66-NO₂ (3) and UiO-66-Br (4) were synthesized analogously by replacing H₂BDC with the equivalent molar amounts of H₂N-H₂BDC, O₂N-H₂BDC and Br-H₂BDC, respectively.

Characterizations

Powder X-ray diffraction (XRD) were recorded with a Bruker D8 Advance X-ray diffractometer operated at 40 kV and 40 mA with Ni-filtered Cu K α irradiation ($\lambda = 1.5406 \text{ \AA}$). UV–vis diffuse reflectance spectra (UV–vis DRS) were obtained by a UV–vis spectrophotometer (Varian Cary 500) with Barium sulfate as a referent. X-ray photoelectron spectroscopy (XPS) measurements were performed on a PHI Quantum 2000 XPS system with a monochromatic Al K α source and a charge neutralizer. The IR experiments were carried out on a Nicolet 670 FT-IR spectrometer. The spectra of samples were collected with diluting by KBr and registered after accumulation of 32 scans with a resolution of 4 cm^{-1} . BET surface area and the N₂ adsorption were carried out on an ASAP2020M apparatus (Micromeritics Instrument Corp., USA). After the samples were degassed in vacuum at 120 °C for 6 h, the nitrogen adsorption and desorption isotherms were measured at 77 K. Electron spin resonance (ESR) signals of spin-trapped paramagnetic species with 5, 5-dimethyl-1-pyrroline N-oxide (DMPO) were recorded with a Bruker A300 spectrometer. A 300 W Xe lamp (PLS-SXE 300, Beijing Perfectlight Co. Ltd.) was used as a light source.

Evaluation of photocatalytic activity

The As(III) solution (1 g/L) was prepared by adding 1.734 g of NaAsO₂ to 1 L 2% HCl solution, and then the solution was diluted with ultrapure water ($18.2 \text{ M}\Omega \text{ cm}^{-1}$) to obtain 2 mg/L As(III) solution. The reaction suspension was prepared by adding 40 mg photocatalyst to 40 mL 2 mg/L As(III) aqueous solution. Prior to illumination, the suspension was stirred for 60 min in the dark to establish an adsorption–desorption

equilibrium. Then the suspension was irradiated by a 300 W Xe lamp. During the oxidation process, 2 mL suspensions were collected and centrifuged every 20 min. Then the supernatant liquids were taken out and detected by Atomic fluorescence spectrometry (PF6, Beijing purkinje general instrument Co., Ltd.) method. The total arsenic concentration was detected by reduction the remaining solution using thiourea and L-ascorbic.²

Potassium dichromate ($K_2Cr_2O_7$) was chosen as a representative Cr(VI) compound. The photocatalytic reaction was carried out at 30 °C in a 100 mL quartz reactor containing 20 mg photocatalyst and 40 mL 10 ppm Cr(VI) aqueous solution. After being stirred for a sufficient amount of time to reach adsorption–desorption equilibrium. The suspensions were irradiated by a 300 W Xe arc lamp (PLS-SXE 300, Beijing Perfectlight Co. Ltd.). During illumination, about 2 mL of suspension was taken from the reactor at a scheduled interval and centrifuged to separate the photocatalyst. The Cr(VI) content in the solution was determined using the diphenylcarbazide (DPC) method.³ The Cr(VI) shows a characteristic peak at 540 nm in the UV-vis absorption curve. The higher the Cr(VI) concentration in the solution, the stronger peak intensity was observed. The measured absorbance intensities at different illumination times were transformed to the reduction ratio of Cr(VI), which is calculated using the following expression:

$$\text{Reduction ratio of Cr(VI)} = (C_0 - C_t) / C_0 * 100\%$$

Where C_0 and C_t are the absorbance intensities when illuminated for 0 (that is, just after the dark adsorption) and t min, respectively.

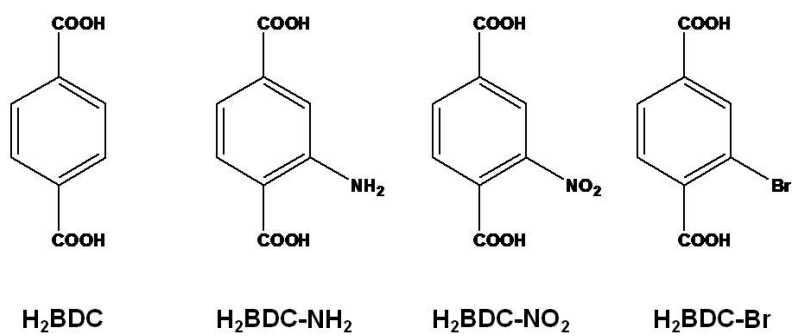


Fig. S1. Functionalised terephthalic acid linker molecules H₂BDC-X used for the synthesis of the UiO-66-X.

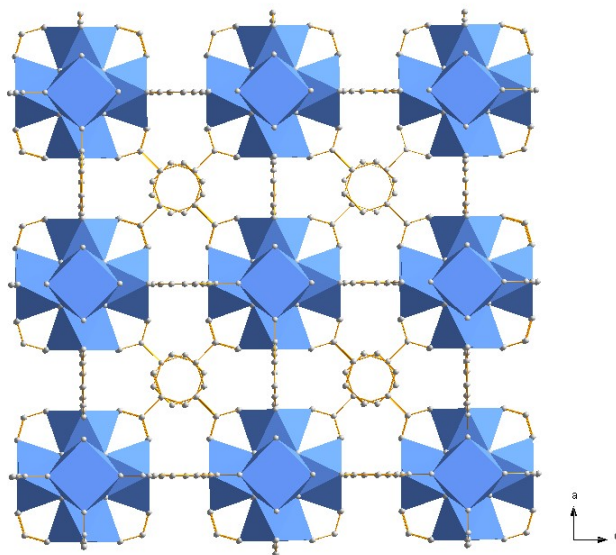


Fig. S2. 3D cubic framework structure of UiO-66.

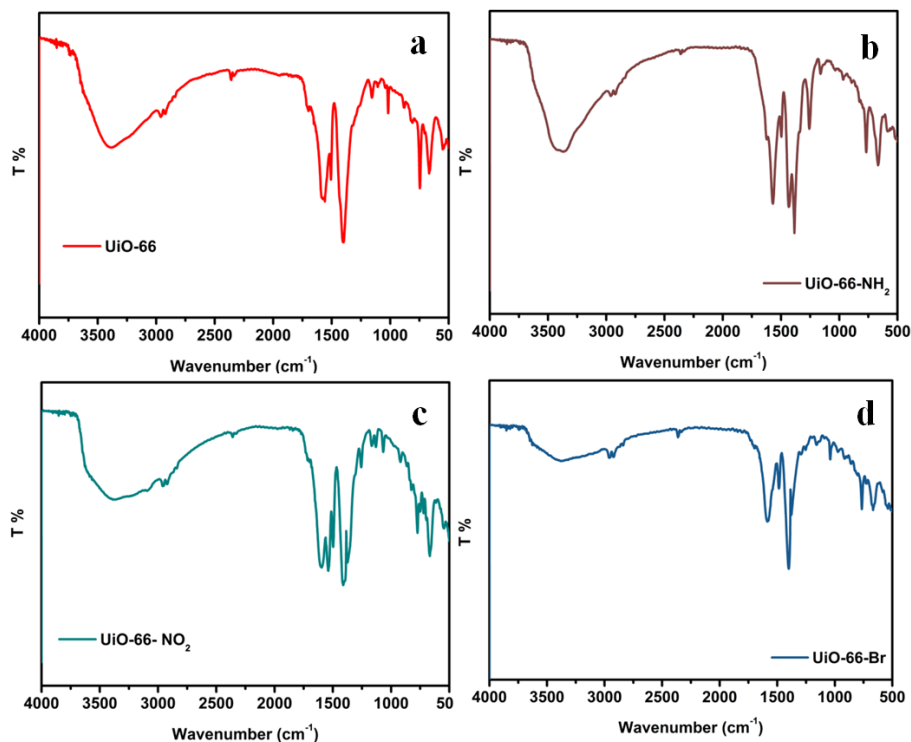


Fig. S3. IR spectra of UiO-66-X: UiO-66 (a), UiO-66-NH₂ (b), UiO-66-NO₂ (c), UiO-66-Br (d).

UiO-66-NH₂ displays two absorptions at 3449 cm⁻¹ and 3362 cm⁻¹ when compared with the IR spectrum of UiO-66, which are ascribed to the asymmetrical and symmetrical stretching vibration adsorption of the amine groups. In the lower frequency region, the peaks center at 1624 cm⁻¹ and 1246 cm⁻¹ correspond to the N-H bending vibration and the characteristic C-N stretching of aromatic amines, respectively.⁴ Fig. 3Sc shows the IR spectrum of UiO-66-NO₂. Focusing on the 1550-1500 cm⁻¹ region, two additional bands can be observed when compared with UiO-66, one is centered at 1539 cm⁻¹ and the other, partially overshadowed by a strong band attributed to a carboxylate mode, appears as a shoulder at approximately 1249 cm⁻¹. These bands can be reasonably ascribed to the NO₂ group.⁵ The IR spectrum of UiO-66-Br is quite similar to the one obtained for UiO-66. Although there are no pure carbon-halogen stretching vibration modes for aromatic halogen compounds, the presence of peaks sensitive to the bromo functionality are evidenced.

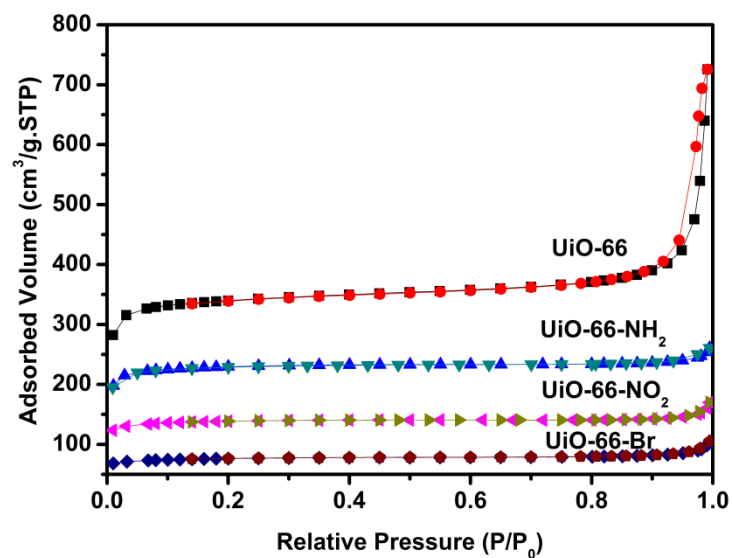


Fig. S4. BET adsorption-desorption isotherms of UiO-66-X.

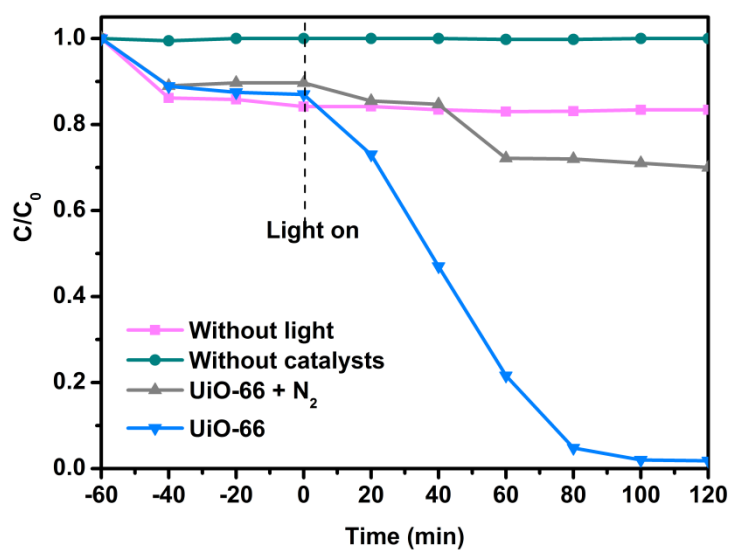


Fig. S5. Reaction process for dark adsorption and photocatalytic oxidation of As(III) over UiO-66. C_0 and C refer to the initial As(III) concentration determined at different reaction time, respectively.

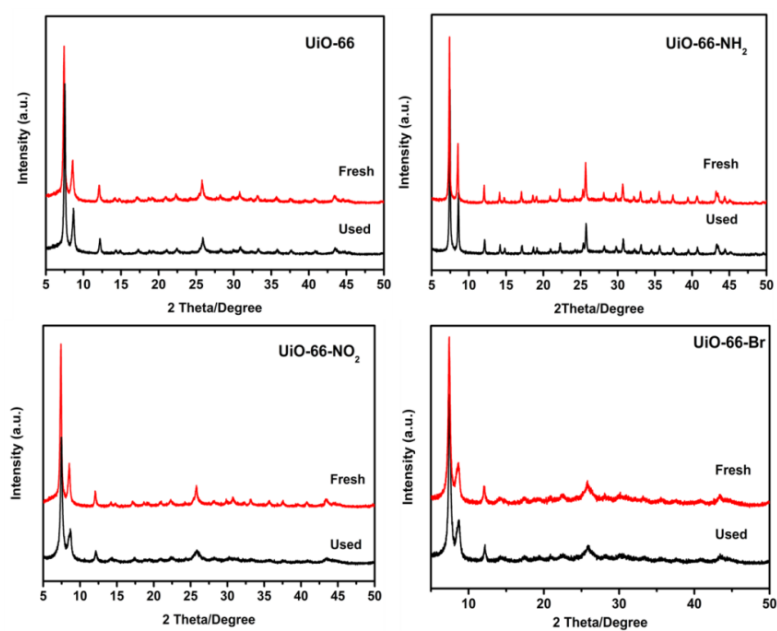


Fig. S6 XRD patterns of UiO-66-X (X=H, NH₂, NO₂ and Br) before and after the photocatalytic oxidation of As(III).

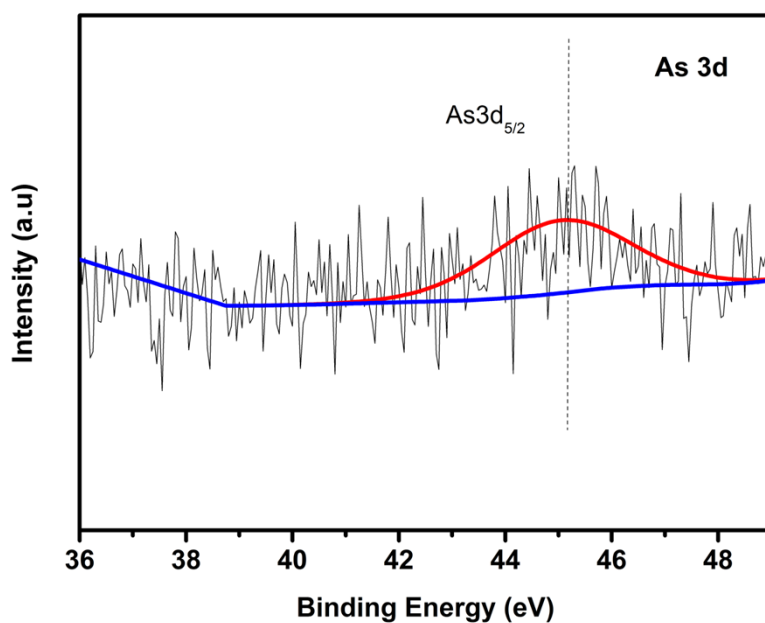


Fig. S7. As 3d XPS spectrum on the surfaces of UiO-66 after photocatalytic oxidation process.

To gain more insight into the reaction, some measures have been taken. X-ray photoelectron spectroscopy has been used to investigate the state of As(III) and As(V).

From **Fig. S7**, it can be seen that the characteristic peaks of As 3d located at 45.5 eV,

which is assigned to As(V),⁶ indicating As(III) can be effectively oxidize, and the resulting As(V) can be adsorbed on the surfaces of UiO-66. To test the reusability of the catalyst system, the used UiO-66 was used in the successive run after washed then dried. As shown in **Fig. S8**, UiO-66 could retain its activity fairly well even after three cycles of application, indicating the high reusability of UiO-66.

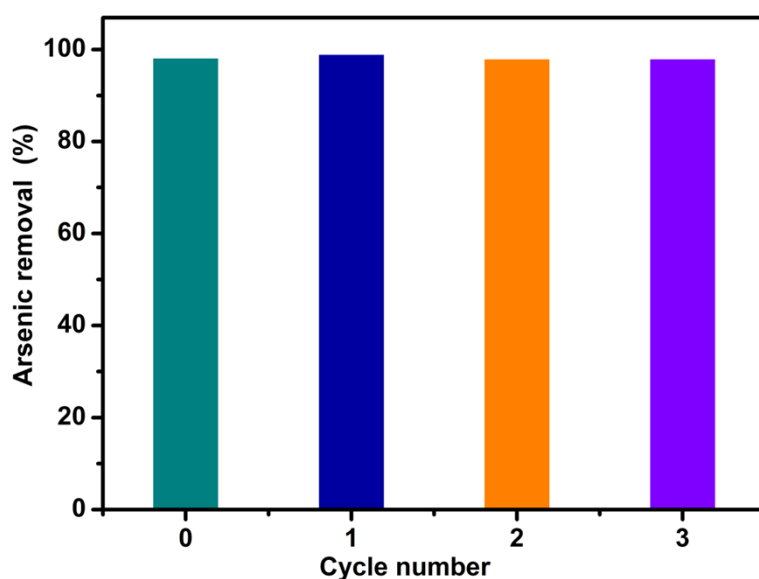


Fig. S8. Reusability of UiO-66 for the photocatalytic oxidation of As(III).

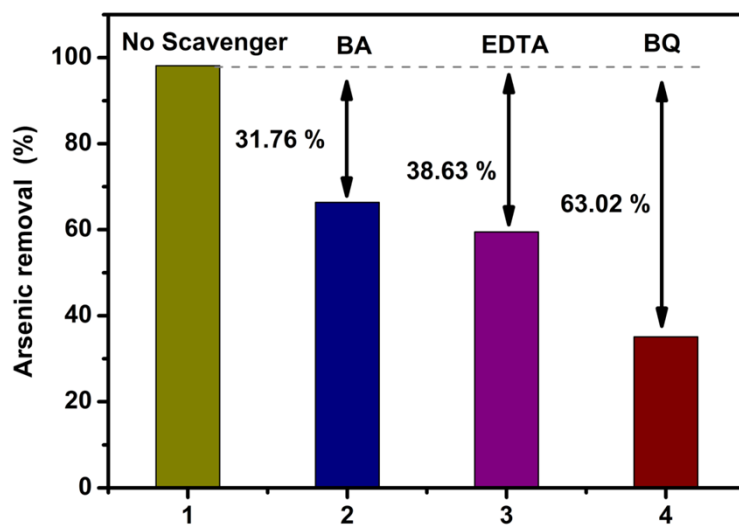


Fig. S9. Photocatalytic oxidation of As(III) over UiO-66 in the presence of trapping

systems (scavenger amount: 15 mg).

To further understand the photoactive species during oxidation of As(III) over UiO-66, quenching experiments with different radical scavengers have been performed. As shown in **Fig. S9**, after adding benzoic acid (BA) for trapping $\bullet\text{OH}$, the photocatalytic oxidation efficiency of As(III) on UiO-66 decreases from 98.1 % to 66.4 %. Moreover, the photocatalytic oxidation of As(III) over UiO-66 is also inhibited when the ethylene diamine tetraacetic acid (EDTA) was added as a hole scavenger. Notably, after adding benzoquinone (BQ) for trapping $\bullet\text{O}_2^-$, the photocatalytic oxidation efficiency of As(III) on UiO-66 decreases significantly, that is from 98.1 % to 35.1%, indicating that the $\bullet\text{O}_2^-$ is an very important active species in this system. To sum up, $\bullet\text{OH}$, h^+ and $\text{O}_2\bullet^-$ are all responsible for the oxidation of As(III) over UiO-66 photocatalyst. In which, the $\text{O}_2\bullet^-$ plays a major role for photocatalytic oxidation of As(III), this is further verified by the electron spin resonance (ESR) measurements in the presence of DMPO. As shown in **Fig. S10**, DMPO- $\bullet\text{O}_2^-$ adducts with six characteristic peaks could be observed in the methanol solvent after the irradiation of light, while in the dark no obvious peaks can be observed. Thus, it is reasonable to infer that $\bullet\text{O}_2^-$ is the main active oxygen species generated to oxidize the As(III) to As(V) in the UiO-66-X photocatalytic system.

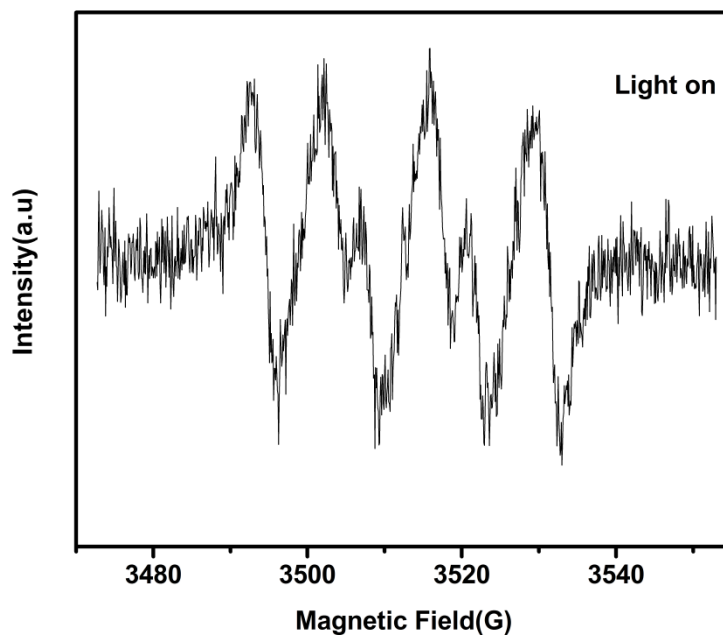


Fig. S10. ESR spectrum of the radical adduct trapped by DMPO (DMPO ··O₂[·]) in CH₃OH over the sample of UiO-66.

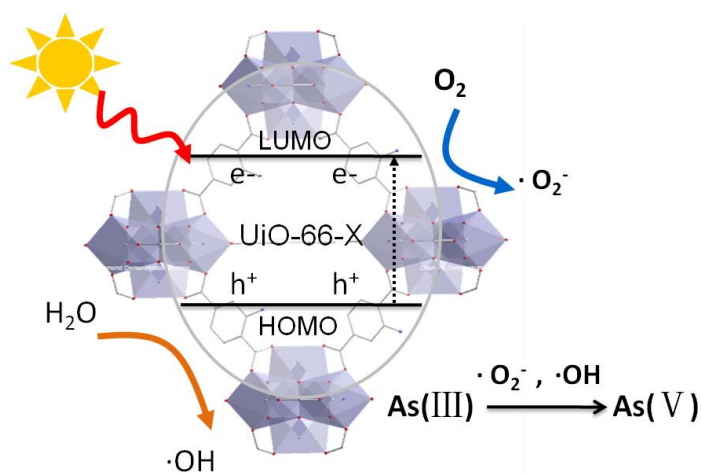


Fig. S11. Possible mechanism of photocatalytic oxidation of As(III) over UiO-66-X.

Base on above discussion, a possible mechanism for photocatalytic oxidation of As(III) over UiO-66 is proposed, as illustrated in **Fig. S11**. The targeted reactants are adsorbed on the surface of our samples. Under light irradiation, the charge carrier has been produced and the photogenerated electrons and holes respectively transferred to

the catalyst's surface quickly. The photogenerated electrons in CB could reduce O_2 to $\bullet O_2^-$ because the E_{CB} of the UiO-66 is more negative than $E_0(O_2/\bullet O_2^-)$ (-0.33 V vs NHE at pH 7).⁷ Since the VB potential (E_{VB}) of UiO-66 is more negative than $E_0(\bullet OH/H_2O)$ (1.97 V vs NHE at pH 7), the photogenerated holes cannot oxidize the hydroxyl groups. Instead, they oxidize the As(III) adsorbed on the surface of UiO-66 directly.

Table S1. Zr $3d_{5/2}$ binding energies for UiO-66 with a wide variety of substituents.

Samples	UiO-66	UiO-66-NH ₂	UiO-66-NO ₂	UiO-66-Br
Zr $3d_{5/2}$ Binding energies (eV)	182.54	182.45	182.72	182.68

Table S2. Summary of specific surface area and the photocatalytic activities of UiO-66-X photocatalysts

Samples	BET (m ² /g)	K [h ⁻¹]	K'[g.h ⁻¹ .m ⁻² , ×10 ⁻⁵]
UiO-66	1141.1	0.0266	2.33
UiO-66-NH ₂	732.2	0.0417	5.69
UiO-66-NO ₂	464.8	0.00369	0.79
UiO-66-Br	455.9	0.0128	2.8

The reaction kinetics of As(III) oxidation were analyzed with the pseudofirst-order model. The k' values were k values normalized with the surface areas.

Reference

1. J. H. Cavka, S. Jakobsen, U. Olsbye, N. Guillou, C. Lamberti, S. Bordiga and K. P. Lillerud, *J. Am. Chem. Soc.*, 2008, **130**, 13850–13851.
2. H. Wu, T. Yildirim and W. Zhou, *J. Phys. Chem. Lett.*, 2013, **4**, 925-930.
3. A. Idris, N. Hassan, R. Rashid and A.-F. Ngomsik, *J. Hazard. Mater.*, 2011, **186**, 629.
4. Y. Lin, C. Kong and L. Chen, *RSC Advances*, 2012, **2**, 6417-6419.
5. M. Kandiah, M. H. Nilsen, S. Usseglio, S. Jakobsen, U. Olsbye, M. Tilset, C. Larabi, E. Quadrelli, F. Bonino and K. P. Lillerud, *Chem. Mater.*, 2010, **22**, 6632–6640.
6. Q. Tian, J. Zhuang, J. Wang, I. Xie and P. Liu, *Appl. Catal. A: Gen.*, 2012, **425-426**, 74-78.
7. Z. Li, T. Dong, Y. Zhang, L. Wu, J. Li, X. Wang and X. Fu, *J. Phys. Chem. C*, 2007, **111**, 4727-4733.